Atmospheric Environment 342 (2025) 120924

Contents lists available at ScienceDirect

Atmospheric Environment

journal homepage: www.elsevier.com/locate/atmosenv

Enhancing Uncrewed Aerial Vehicle Techniques for Monitoring Greenhouse Gas Plumes at Point Sources

Horim Kim [a,b,1], Keun Taek Kim [a,1], Sangjae Jeong [c,*], Young Su Lee [d], Xin Zhao [a], Jae Young Kim [a,**]

[a] Department of Civil and Environmental Engineering, Seoul National University, Seoul, Republic of Korea
[b] Institute of Construction and Environmental Engineering, Seoul National University, Seoul, Republic of Korea
[c] Department of Civil and Environmental Engineering, Hanbat National University, Daejeon, Republic of Korea
[d] Department of Energy and Environmental Engineering, Soonchunhyang University, Asan, Republic of Korea

GRAPHICAL ABSTRACT

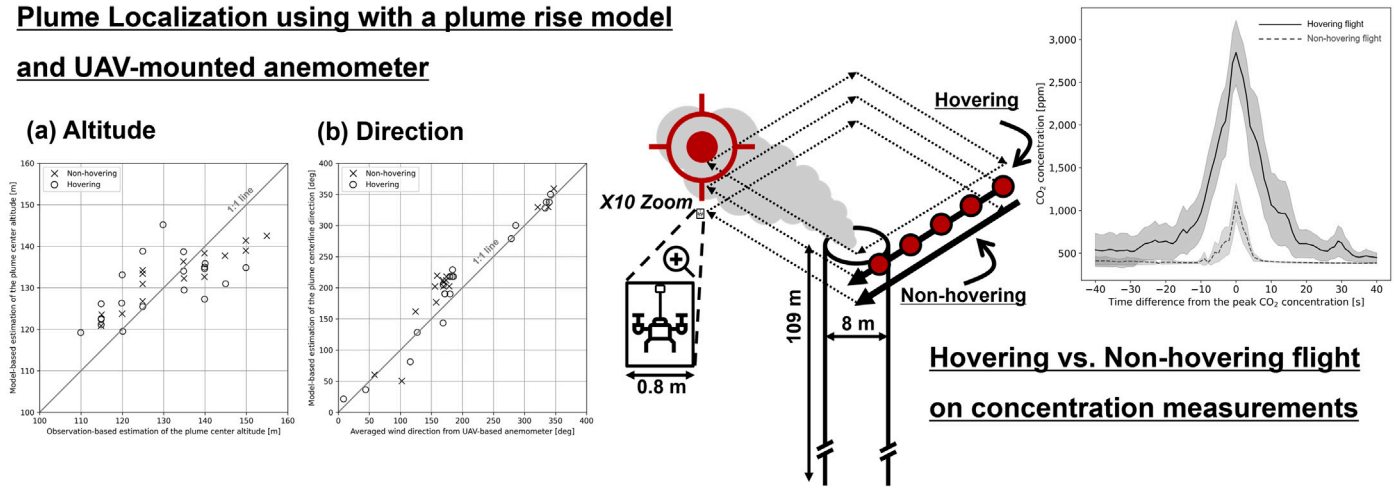

HIGHLIGHTS

- A UAV-mounted anemometers and a plume rise model improve plume localization accuracy.
- Pre-planned autopilot flights enhance measurement efficiency and data reliability.
- Hovering flights capture higher pollutant concentrations than non-hovering flights.
- Multiple UAV-mounted sensors reveal disparities in response times for pollutants.
- A hybrid UAV strategy enhances plume detection and pollutant measurement.

ARTICLE INFO

ABSTRACT

* Corresponding author at: Department of Civil and Environmental Engineering, Hanbat National University, Daejeon, Republic of Korea.
** Corresponding author at: Department of Civil and Environmental Engineering, Seoul National University, Seoul, Republic of Korea.
E-mail addresses: sangjae.jeong@hanbat.ac.kr (S. Jeong), jaeykim@snu.ac.kr (J.Y. Kim).
[1] These authors are equal contributors to this work and are designated as co-first authors.

https://doi.org/10.1016/j.atmosenv.2024.120924
Received 8 July 2024; Received in revised form 7 November 2024; Accepted 8 November 2024
Available online 16 November 2024

Keywords:
UAV monitoring
Plume localization
Point emission source
Air pollutant sensors
Hovering flight

The urgency of the global climate crisis necessitates advanced monitoring of greenhouse gases, with an emphasis on capturing their spatial and temporal variability. This study explores techniques to enhance plume detection and concentration measurements using uncrewed aerial vehicles (UAVs) for monitoring at point sources, specifically at an incineration stack. Through preliminary site investigations, our approach employed strategically designed flight paths and an autopilot system to optimize flight operations within the constraints of limited flight time due to battery capacity. We combined a UAV-mounted anemometer with a plume rise model to localize the plume center at a distance of 30 m from the stack center and evaluated its performance by comparing the model-based estimations at different altitudes and angular directions with the observation results. The comparison demonstrated that the results obtained by localizing the plume center using a plume rise model and a UAV-mounted anemometer aligned well with observations based on CO_2 concentration analysis. The comparative analysis showed a RMSE of 8.44 m and a MAE of 7.26 m for altitude, and a RMSE of 32.31° and a MAE of 25.78° for angular direction. Furthermore, we assessed the effectiveness of hovering UAV flights, in which a UAV remains stationary at a fixed point in the air, compared to non-hovering flights in capturing pollutant concentration. While both methods performed similarly in detecting the plume center, non-hovering flights underestimated the CO_2 concentration due to insufficient time for measurement despite a sensor response time of less than three seconds. Overall, our proposed hybrid monitoring strategy integrates non-hovering and hovering flights, enhancing both plume detection efficiency and concentration measurement accuracy at point sources.

1. Introduction

The global climate crisis, as evidenced by the alarming rise in severe weather events, has worsened despite longstanding scientific warnings (Ripple et al., 2022). The main reason for this is the anthropogenic emission of greenhouse gases (GHGs), which increased from 21 to 59 $GtCO_2$-eq between 1990 and 2019 (Lee et al., 2023). The Intergovernmental Panel on Climate Change (IPCC) guidelines for national GHG inventories (IPCC, 2006) provide a framework for estimating GHG emissions across various industrial facilities. Although sector-specific inventories have been employed, calculation-based estimates for GHG emissions have faced criticism due to their uncertainties, highlighted by comparative analyses with actual measurement data (Newman et al., 2016; Bergamaschi et al., 2015; Chen et al., 2022; Lu et al., 2022a). Given this limitation, validating existing inventories through GHG observation campaigns is essential to better understand their environmental impacts.

Uncrewed aerial vehicles (UAVs), capable of real-time spatially-extensive monitoring, have emerged as versatile tools. With the recent advancements in technology, UAVs can capture the spatial and temporal variability of GHG emissions and estimate the flux from industrial facilities (Brown et al., 2023; Han et al., 2024; Zhao et al., 2024), environmental infrastructures (Gålfalk et al., 2021), nature sources (Rüdiger et al., 2018), and agricultural sources (Vinković et al., 2022). However, discrepancies arise between inventory-based calculations and UAV-based monitoring results mainly due to the differences in the resolution of spatial and temporal data, assumptions made in inventory calculations, and the dynamic nature of emission sources. Han et al. (2024) quantified the emission rates from a coking plant in China, revealing that the values recorded using UAV-measured methane emissions were four times higher than those estimated using the IPCC Tier-1 emission factor. Similarly, Brown et al. (2023) identified the differences between UAV measurement results and inventory estimates at natural gas facilities in the United States, highlighting underestimations in inventory-based approaches.

While utilizing UAVs in GHG emission monitoring has opened up new opportunities, several challenges still remain. One of the primary challenges is the accuracy of pollutant concentration measurement, which is a critical step before reliable emission quantifications can be performed. Several studies encountered difficulties in effectively capturing plumes, resulting in significant discrepancies between measured emissions and inventory estimates (Reuter et al., 2021; Vinković et al., 2022). In response to this challenge, the need for effective plume detection must be highlighted. Another challenge is the scale difference between the drone and field site. UAVs, typically less than 1 m in size, operate in environments that span several hundred meters. This disparity complicates precise plume detection and concentration measurement.

Additionally, UAV sensor limitations and battery constraints impact the effectiveness of monitoring campaigns. Researchers noted that the limited payload capacity of UAVs necessitates the use of lightweight, fast-response, and low-power consumption instrumentation, which can impact the measurement accuracy (Burgués and Marco, 2020; Reuter et al., 2021). Other researchers underlined that the accuracy of these types of equipment contributes to the uncertainties in plume measurements (Mønster et al., 2019; Andersen et al., 2021).

A notable gap in the current research on UAV-based monitoring is the absence of standardized protocols and evaluation criteria. Ma et al. (2021) highlighted the ongoing need for developing practical guidelines for scientifically meaningful sampling using UAVs, including optimization strategies for sampling height and duration to meet specific scientific objectives of each study. Andersen et al. (2021) also emphasized the importance of structured flight planning for quantifying methane emissions from a point source in a coal mining area. Our research addresses this gap by introducing a novel methodology that enhances UAV technology for GHG monitoring with improved measurement efficiency. Guided by preliminary site investigations, our study developed pre-planned flight paths to conduct measurements, utilizing an autopilot system to refine these paths further. The designed flight routes included boundary flights around the incinerator stack, with horizontal distances of 30 meters from the stack center and vertical intervals of 5 meters between each layer. These flight routes allowed for efficient use of UAV flight time and enabled the collection of reliable data through repeated experiments.

By integrating a UAV-mounted anemometer anemometers with a plume rise model, the current approach facilitates the effective detection of emission plumes from point sources like incineration plants. A point source was chosen as the research focus because it provides a simpler environment to check the feasibility of model-based plume localization and to validate the model with well-defined emission parameters. Gålfalk et al. (2021) highlighted the importance of a UAV-mounted anemometer and revealed that a UAV-mounted anemometer can capture temporal and spatial variability with higher resolution than a ground weather station. Han et al. (2024) and Reuter et al. (2021) also utilized onboard anemometers, emphasizing the significance of acquiring meteorological information along the flight route. The performance of the UAV-mounted anemometer was further examined by comparing it with that of a ground-based weather station, which has often been utilized for wind data estimation in previous studies in this field of study (Allen et al., 2019; Shah et al., 2020). Moreover, we investigated the benefits of hovering flight modes, defined as the condition in which a UAV remains stationary at a fixed point in the atmosphere (Oosedo et al., 2017). Our study examined the effect of hovering flights on concentration measurements, regarding that it allows sensors more time to capture concentration. Furthermore,

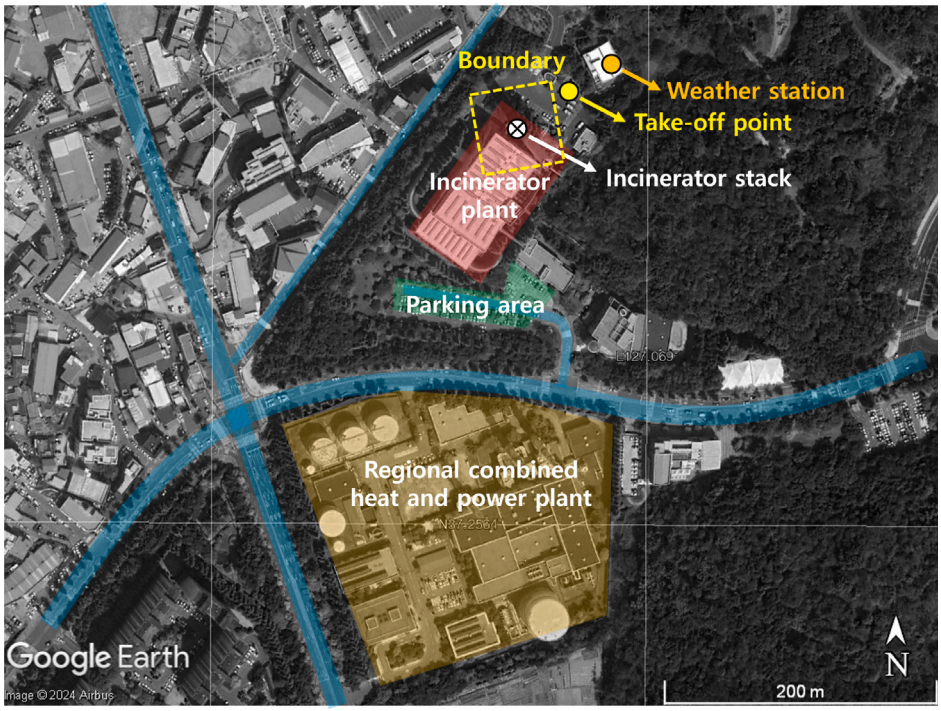

Fig. 1. Geographical location of the investigated incinerator plant and its surroundings. The blue-colored lines depict the local road networks, and the yellow-colored region illustrates the site of a regional combined heat and power plant nearby. The map was obtained from Google Earth Pro (Google Earth Pro 7.3.6.9750, 2024).

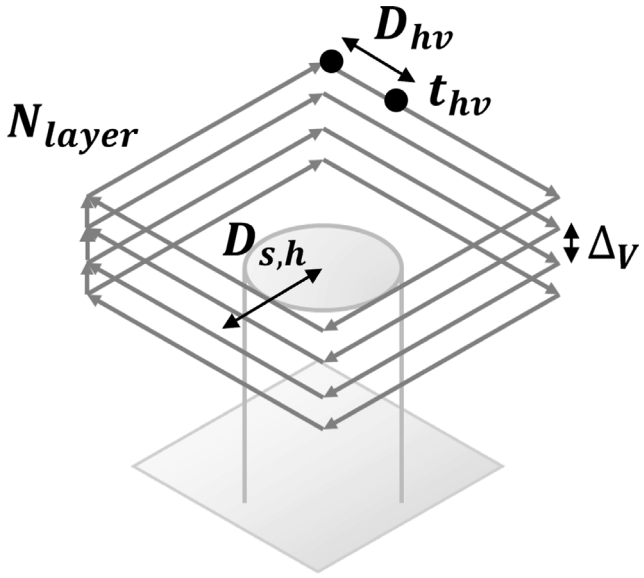

Fig. 2. A schematic representation of a boundary flight mission around the incinerator stack. The key factors of the flight routes are presented in Table S2.

we examined the role of sensor responsiveness to pollutants during UAV-based monitoring, a topic not widely explored in existing literature. This study aimed to understand how different sensor response times impact the effectiveness of pollutant detection during UAV field campaigns.

2. Materials and methods

2.1. Field campaign

The field campaigns were conducted at an incineration facility located in the southern region of Gyeonggi Province, part of the Seoul metropolitan area. The incineration plant is a significant source of air pollutant emissions, including greenhouse gases, particulate matter, and gaseous pollutants (U.S. Environmental Protection Agency, 2024). The specific site was selected because incinerator plants are well-recognized sources of CO_2 (UNFCCC, 2007), and the facility operates nearly year-round, providing good feasibility for implementing field experiments. The facility processes 400 to 600 metric tons of municipal solid waste per day using stoker-type incinerators. In addition, the stack height is 109 m, and the diameter of the emission gas outlet is about 1.6 m. The scale difference between the drone and the field site is illustrated in Note S1 in the supplementary information (SI).

As depicted in Fig. 1, the incinerator plant is located in a complex urban landscape, surrounded by local road networks, a parking lot, and a regional combined heat and power plant equipped with emission stacks. For such an environment, with various potential pollution sources and diverse terrain, we require a careful strategy to isolate the targeted emissions from other sources and to deal with the city's complex geography. The impact of urban structures on pollutant dispersion has been identified in previous research (Villa et al., 2017; Kuuluvainen et al., 2018; Park and Lee, 2024). Therefore, flight operations for concentration measurements in this study were executed as close to the point source (incinerator stack) as possible to minimize the impact of surrounding pollutant sources on the measurements. In addition, we implemented a boundary flight mission during the field campaign, which measured the concentrations on all four sides of boundary squares near the stack (Fig. 1), rather than just the two sides (downwind and upwind) of the plume.

The field campaigns were was implemented over five distinct days between September and December 2023. UAV flight operations were conducted during the daytime, typically from 9 AM to 5 PM. The operations were restricted to the daytime due to legislative permissions. Table S1 in SI Note S4 summarizes the environmental conditions for each day of the campaigns.

2.2. Preliminary investigations for UAV flight operation design

Before the main field campaigns, a preliminary investigation was performed to achieve two objectives: (1) to obtain practical information

for UAV flight missions at the target site and (2) to gather the data necessary for designing autopilot flight routes. The take-off point was determined (see SI Note S3 for selection criteria) as marked by a yellow dot in Fig. 1.

Initially, the UAV was manually operated around the incinerator stack to identify key factors for the autopilot setup (Table S2). These factors primarily focused on managing battery constraints and ensuring flight safety. Safety considerations are required to determine the minimum safe distances from the incinerator stack. Given that the exit gas temperatures from the stack were approximately 180 °C, establishing a safe operational distance was crucial to protect the UAV and its sensors from the high-temperature emissions. The distance from the stack center for the flight mission (see the scheme in Fig. 2), $D_{s,h}$, was set to 30 m, balancing the UAV's battery life limitations and safety concerns regarding the high temperatures of the exiting gas. Through manual flight missions, we found that flight operations closer than this distance resulted in sensor temperatures exceeding 40 °C, posing a potential risk to the equipment.

In addition, due to the UAV's limited flight time, the feasible number of data collection layers (N_{layer}) and their vertical interval (Δ_V) had to be examined. The vertical interval Δ_V was set at 5 m, considering the σ_z values derived from Pasquill-Gifford (PG) coefficients within the Gaussian plume dispersion parameter correlations (Seinfeld and Pandis, 2016). With UAV flights predominantly conducted under conditions corresponding to stability classes A and B during the daytime (see Table S1 in SI Note S4), Δ_V was selected to be less than twice the σ_z value for both classes to ensure plume detection within the vertical gaps. A 5 m interval was chosen to capture the plume's centerline at a 30 m distance to ensure high likelihood of detection; a larger interval might fail to accurately detect the centerline.

In this study, two different flight modes, hovering and non-hovering, were executed for the field campaign. A few previous studies, such as Alvarado et al. (2017) and Kuantama et al. (2019), explored the hovering flight for improving accuracy in particulate and gas concentration monitoring. However, comparative studies directly examining the effectiveness of hovering and non-hovering flight modes under the same monitoring conditions remain limited. Thus, a part of this study addressed this gap by examining the performance of UAVs in this context. The present study analyzed both flight modes, evaluating 20 hovering flight missions and 15 non-hovering flight missions conducted at the targeted sites. A total of 35 flight missions were selected from 45 flight operations based on the validation criterion for the CO_2 concentrations, as described in Section 2.4.2. For non-hovering flights, the UAV required approximately 9 min to complete nine layers ($N_{layer} = 9$) of monitoring within the given boundary, from 110 m to 150 m. This altitude range was set based on the plume center altitude range calculated using Brigg's plume rise model (Briggs, 1984) at a horizontal distance ($D_{s,h}$) of 30 m with wind speeds of 2 to $8\,m\,s^{-1}$. The N_{layer} value for hovering flight missions was set at 3, considering the number of missions that can be executed for the maximum flight duration (around 25 min) with one battery set. For hovering flights, the distance between hovering points (D_{hv}) was 10 m, and the time spent at each hovering point (t_{hv}) was 10 s. D_{hv} was determined by considering the lateral dispersion coefficient, σ_y, from the Pasquill-Gifford (PG) coefficients to optimize lateral plume detection. Both D_{hv} and t_{hv} were chosen to balance the need for accurate plume detection with the limited flight duration per mission using a single battery set. The location of hovering points was specified when mapping autopilot routes using Google Earth Pro to ensure precise positioning. During the data analysis, hovering status was determined by analyzing the UAV's displacement. Considering possible subtle movements due to wind or operational influences, a period was categorized as hovering when the UAV's movement stayed below 20 centimeters per second, signifying stable positioning.

In traditional monitoring methods, manually navigating drones are often employed around emission sources without a specific target area for the plume, which may lead to inefficient use of UAV flight time and reduced data comprehensiveness and precision. To address this issue, autopilot flight routes were created using Google Earth Pro and the DJI 'Pilot 2' app in the current research. Detailed information regarding the execution of autopilot operations can be found in the SI Note S5.

2.3. Measurement instrumentation

We employed the DJI Matrice 300 RTK, produced by DJI Technology Inc. (Figure S2). The drone can carry a payload of up to 2.7 kg. Although its specifications suggest a maximum flight duration of 55 min, practical operations with sensor system payloads, considering flight safety, limit flight times to approximately 25 min. In addition, wind conditions significantly influenced UAV operations; although the UAV can be operated at wind speed of up to $15\,m\,s^{-1}$ according to its specifications, a conservative wind speed threshold of $10\,m\,s^{-1}$ was set for safety. Detailed information regarding the UAV specifications can be found in the SI Note S2.1.

The current study utilized a custom-developed onboard sensor system from Soarability Technology LLC (Shenzhen, China). The system features four sensor modules: an onboard sonic anemometer module, a non-dispersive infrared (NDIR) CO_2 sensor module, a tunable diode laser absorption spectroscopy (TDLAS) CH_4 sensor module, and a *Sniffer4D V2* module containing electro-chemical sensors for gaseous pollutants (VOCs, CO, NO_2, O_3 and H_2S) and a laser-based sensor for particulate matter ($PM_{1.0}$, $PM_{2.5}$, PM_{10}). The modules are also manufactured by Soarability Technology LLC (Figure S3 and Table 1). For detailed specifications of the UAV and the sensor modules, refer to the SI Note S2.2. Although the system was designed for multiple purposes, including exploring diverse environmental infrastructures such as incineration plants, wastewater treatment plants, and landfill sites, the present study primarily focused on monitoring CO_2 plume emissions from the incinerator stack.

In addition, we examined the usability of wind speed and direction data from a ground-based weather station in model-based estimation. Previous research often relied on downwind plume measurement techniques, frequently estimating plume direction by acquiring wind data from ground-based weather stations (Allen et al., 2019; Shah et al., 2020). In this study, the wind measurements by a UAV-mounted sonic anemometer were compared with those from ground-based weather stations to examine the effectiveness of each method in estimating the wind properties for point source localization. The weather station was situated 10 m above ground level, and adjustments were made to the weather station's data to estimate wind speeds at the incinerator stack's height (109 m) using the wind profile power law (Eq. (1)) with a power coefficient (α) of 0.15 (U.S. Environmental Protection Agency, 1995). The coefficient value was selected considering that all flight missions took place in urban areas under atmospheric stability classes A or B.

$$u_s = u_{\text{ref}} \cdot \left(\frac{h_s}{z_{\text{ref}}} \right)^{\alpha} \quad (1)$$

where:
u_s is the wind speed at stack height,
u_{ref} is the observed wind speed at the ground station,
h_s is the stack height,
z_{ref} is the wind measurement height at the ground station.

The Vantage Pro2 weather station (Davis Instruments, Hayward, CA, USA) was used to gather meteorological data from the ground, primarily the wind speed and direction. The station was installed on the roof of a building at the plant (10 m above ground level), positioned approximately 75 m horizontally from the incinerator stack, marked by an orange dot in Fig. 1. Further details regarding the weather station are provided in SI Note S2.3.

Table 1
The specifications of sensor modules used in the study: including measurement ranges and resolution for wind speed, wind direction, CO_2 sensor, and CH_4 sensor. Further details on the capabilities of the Sniffer4D V2 are available in the SI Note S2.2.

Module	Metrics	Measurement range	Resolution
Sonic anemometer	wind speed	0–50 $m\,s^{-1}$	0.1 $m\,s^{-1}$
	wind direction	0–360°	1°
NDIR sensor	CO_2	0–2,000 ppm	1 ppm
TDLAS sensor	CH_4	0–15,000 ppm	1 ppm
Sniffer4D V2	GPS coordinates, environmental parameters , and various gaseous and particulate pollutants	Refer to SI Note S2.2	

2.4. Model-based and observation-based estimation of localize the plume centerline

2.4.1. Model-based estimation of plume centerline altitude

The model-based calculations for estimating the plume centerline altitude were performed using Briggs' plume rise model (Briggs, 1984). The model adopted in this study is from the AERMOD atmospheric dispersion modeling system (Version 23132), which was used to calculate the plume rise (Δh_d) in the convective boundary layer (CBL) (U.S. Environmental Protection Agency, 2023). The CBL condition was regarded because all flight operations were conducted during the daytime. The model considers the effects of source momentum (F_m) and buoyancy (F_b), detailed in Eq. (2).

$$\Delta h_d = \left(\frac{3F_m x}{\beta_1^2 u_p^2} + \frac{3}{2\beta_1^2} \cdot \frac{F_b x^2}{u_p^3} \right)^{\frac{1}{3}} \quad (2)$$

where:
x represents the distance from the stack center, set at 30 m for this study,
$F_m = \left(\frac{T}{T_s}\right) \cdot w_s^2 \cdot r_s^2$ is the stack momentum flux,
$F_b = g \cdot w_s \cdot r_s^2 \cdot \left(\frac{T_s - T}{T_s}\right)$ is the stack buoyant flux,
β_1 is the entrainment parameter, set to the default value of 0.6 as described in the AERMOD documentation (U.S. Environmental Protection Agency, 2023),
u_p corresponds to the wind speed at the stack height.

The wind speed (u_p) and ambient temperature (T) were derived from the sensor modules for each flight mission. To determine F_m and F_b, operational data from the incinerator stack's monitoring system provided information regarding exit gas temperature (T_s) and gas flow velocity (w_s). The monitoring system recorded measured data every 5 min, including exit gas temperature (T_s), gas flow rate (Q_{gas}), and the concentrations of six components: O_2, NO_x, SO_x, CO, HCl, and total suspended particles. CO_2 concentration data, which is a major focus of this study, was not measured by the system. Q_{gas} was used to calculate the gas flow velocity (w_s) with the formula $Q_{gas}/(\pi r_s^2)$, where the stack radius (r_s) is 0.8 m. The gravitational acceleration (g) was set to 9.81 $m\,s^{-2}$. These values were used to estimate the plume rise across various wind speeds, enabling the estimation of the plume centerline altitude at a distance of 30 m from the incinerator stack. The estimations for each flight mission were conducted using the averaged values of relevant parameters recorded during that mission.

2.4.2. Observation-based estimation of plume characteristics through CO_2 concentration data analysis

CO_2 concentration data were chosen to experimentally determine the plume centerline. This method was selected based on two factors: (1) CO_2 is notably released from the incinerator stack (U.S. Environmental Protection Agency, 2024), and (2) the NDIR CO_2 sensor utilized in the present study offers relatively better specifications for detecting the plume's center than low-cost electro-chemical sensors, including a shorter response time and a wider detection range. Moreover, CH_4 emissions are considered a trivial concern of the incinerator stack (Bogner et al., 2008).

Valid flight missions were selected based on CO_2 concentration criterion to confirm that a mission detected the plume center. Based on insights gained from the results of field measurements and analysis, the criterion was established for valid concentration measurement missions by considering the continuous emissions from the point source and detection thresholds. A flight mission was considered valid if it recorded a peak CO_2 concentration at least double the average background level (390–420 ppm), resulting in a threshold of around 800 ppm for plume center detection. This threshold aligns with Gaussian plume model-based calculations (detailed in the SI Note S7), where the model calculation of plume center concentration is typically above 1,000 ppm. Flights classified as "invalid" in this study had peak CO_2 concentrations averaging 488 ppm, indicating they likely did not detect the plume center. Given the consistent emissions from the point source, we attributed these invalid flights to missed plume detection. Therefore, 35 out of 45 flight missions were selected as valid and were used for the analysis.

2.5. Statistical analysis

Statistical analysis was applied to interpret the sensor data, facilitating comparison and characterization of model-based estimations against observational results of plume localization. The analysis examined two statistical metrics, the root mean square error (RMSE) and the mean absolute error (MAE). Detailed formulations for these metrics are provided in Table S3 in SI Note S6. Both RMSE and MAE were used to compare the effectiveness of the model-based estimation values against observation-based estimation values. A higher RMSE indicates a wider spread of errors, highlighting substantial deviations of model estimations from the observation values, whereas the MAE reflects the average error magnitude. The key difference between the two metrics is that RMSE gives more weight to larger errors, emphasizing significant discrepancies, whereas the MAE provides a straightforward average error across all comparisons. These metrics helped evaluate the new approach introduced in the present study, which was used to localize the plume centerline based on the plume rise model and wind data from the UAV-mounted anemometer.

3. Results and discussion

3.1. Localizing the plume centerline with a plume rise model and a UAV-mounted anemometer

A comparative analysis of model- and observation-based estimations was conducted to evaluate the effectiveness of the plume rise model and UAV-mounted anemometer in determining the location of the plume center. The plume center's altitudes for each flight mission were derived from Briggs' plume rise model using wind speed data from the UAV-mounted anemometer as detailed in Section 2.4.1. The direction of the plume centerline was estimated by averaging the wind direction data recorded by the UAV-mounted anemometer for each flight mission. These estimated values were then compared with the observational location of the maximum CO_2 concentration data.

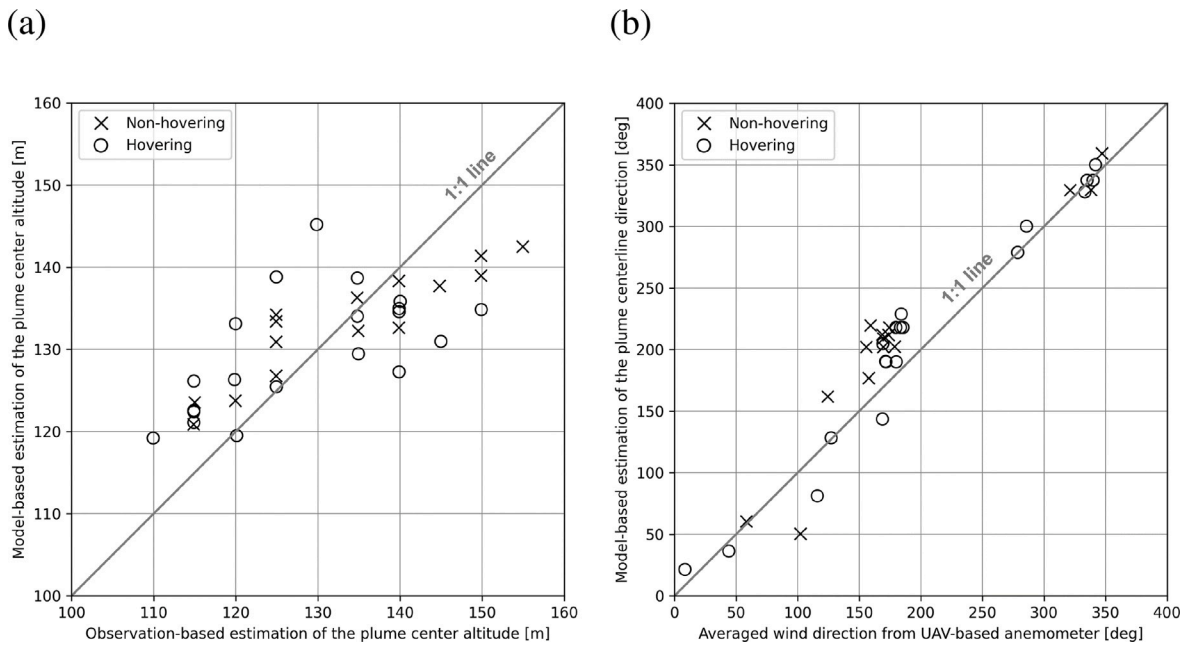

Fig. 3. Comparison of model- versus observation-based estimations of plume characteristics at 30 m from the incinerator stack. Figure (a) illustrates the altitude comparison of the maximum CO_2 concentration data points from each flight mission with the plume-rise model's calculated altitude of the plume center. Figure (b) compares the direction of the maximum CO_2 concentration data points to the average wind direction measured by the UAV-mounted anemometer.

Fig. 3(a) illustrates the correlation between the estimated values calculated from the plume-rise model and the experimental observations of the plume center's altitude. The statistical metrics, with a RMSE of 8.44 m and a MAE of 7.26 m (see Table 2), confirm that the model-based estimation aligned well with the observational values and demonstrated the reliability of the model. The ability of the UAV-anemometer data to estimate the plume's trajectory direction is also described in Fig. 3(b), with RMSE and MAE values of 32.31° and 25.78°, respectively. These values indicate that the accuracy of direction estimation was comparable to that of altitude estimation.

In contrast to the estimation using wind data from the UAV-installed anemometer, the estimated plume centerline characteristics derived from weather station data, as shown in Fig. 4, demonstrated weak correlations with the observational location of the plume center. As shown in Table 2, for altitude, the notably large RMSE of 1,270.45 m and MAE of 548.60 m indicate the severe limitations of weather station data in estimating the altitude of the plume center. The weather station data also showed limited performance in estimating wind direction, with an RMSE of 113.92° and an MAE of 103.02°.

These findings highlight the advantages of a UAV-mounted anemometer over a ground-based weather station in providing reliable data for plume detection. Acquiring qualified wind data at the point source location is crucial for accurate plume localization; however, the weather station was inadequate for precise plume localization. Two main reasons for this inadequacy are first, near-surface turbulence can distort accurate wind speed measurements, resulting in discrepancies between the actual wind speed at the height of the stack and the estimates obtained using the wind profile power law (Finn et al., 2018; Li and Yu, 2018). During some flight missions, wind speeds measured by the ground station were as low as $0.1\,m\,s^{-1}$, likely due to local turbulence and the complex topography of the field site. When these low wind speeds were applied to Briggs' plume rise model, they resulted in unusually high plume centerline heights (above 1,000 m). Second, the complex topography of urban areas can significantly alter ground station measurements, potentially introducing errors in the assessment of both wind speed and direction (Lu et al., 2022b; Sekula et al., 2021). Using a constant power coefficient of 0.15 for the wind power law also introduced potential uncertainty, as it did not account for turbulence or meteorological conditions such as temperature and pressure variations. Given these challenges, employing UAV-mounted anemometers with the plume rise model enhances the efficiency of plume detection, especially in urban environments with complex emission sources and varied topographies that influence pollutant dispersion.

3.2. Hovering flight and concentration measurement

In the previous section, Fig. 3 and the statistical metrics in Table 2 demonstrate that no significant differences exist in each flight mode's ability to localize the plume centerline. This suggests that for flight missions focused solely on plume detection, opting for non-hovering flight operations could be a more time-efficient choice, as non-hovering flights require only 3 min to move around three layers, whereas hovering flights take 25 min. However, analyses of the CO_2 concentration revealed a benefit in concentration measurements for hovering flights. The hovering flights consistently demonstrated higher peak CO_2 concentrations than non-hovering flights. Fig. 5(a) reveals that the mean values of the peak CO_2 concentration from 15 hovering flight missions reached 2,726.5 ± 960.6 ppm, which is approximately twice the mean values of 1,392.4 ± 526.0 ppm recorded for 20 non-hovering flight missions. This discrepancy is further supported by the time-series data shown in Fig. 6, indicating that sensors in non-hovering flights did not capture as high concentrations as those in hovering flights. The concentration peaks during non-hovering flights appeared to be narrower, suggesting that these flights might not provide adequate time for capturing high concentrations of pollutants.

The discrepancy in CO_2 concentration measurements between hovering and non-hovering flights further suggests that flight speed plays a key role in capturing pollutant concentrations. In particular, flight speed directly affects the time the UAV spends within the plume, which influences sensor response and measurement accuracy. This observation aligns with the perspective that operating at a slower speed during non-hovering flights could improve the ability to capture higher CO_2 concentrations. A slower speed allows the UAV to spend more time within the plume, providing the sensor with sufficient response time. However, while a reduced speed may enhance sensor performance, it also decreases the spatial coverage due to the limited flight duration of

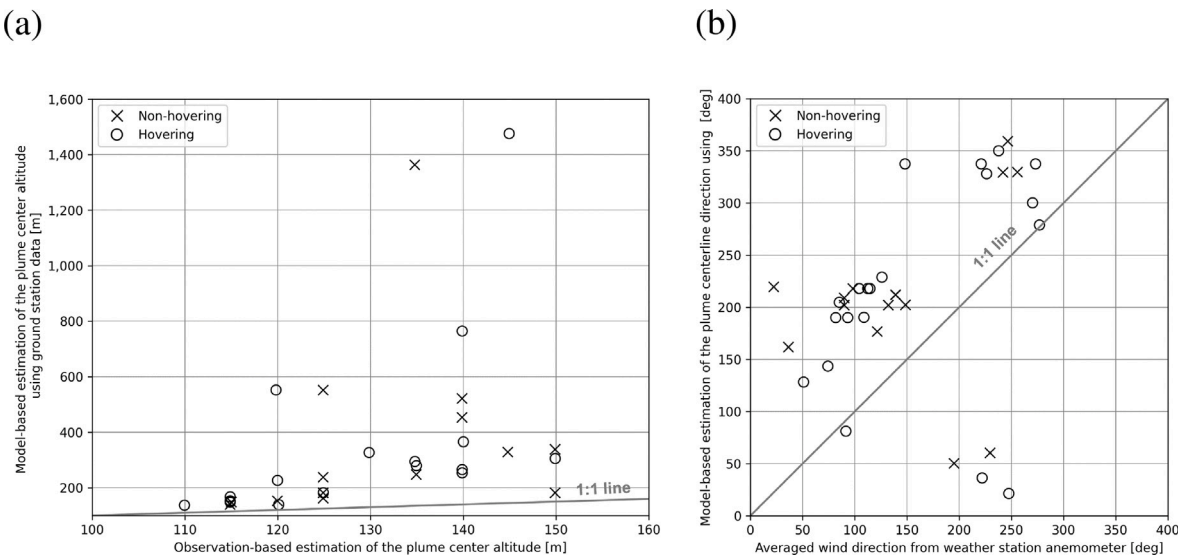

Fig. 4. Comparison of model- versus observation-based estimations of plume characteristics at 30 m from the incinerator stack. Here, wind data were obtained from the ground weather station and utilized to calculate the plume rise. Figure (a) illustrates the altitude comparison of maximum CO_2 concentration data points from each flight mission with the plume-rise model's calculated altitude of the plume center. Figure (b) compares the direction of the maximum CO_2 concentration data point to the average wind direction measured by the ground station.

Table 2
Statistical metrics from the comparative analysis of model-based and observation-based plume characteristics for different flight modes (hovering and non-hovering), as shown in Figs. 3 and 4.

Wind data source: UAV-installed anemometer						
Statistical metrics	Altitude [m]			Direction [°]		
	Non-hovering	Hovering	Total	Non-hovering	Hovering	Total
RMSE	7.23	9.25	8.44	35.55	29.65	32.31
MAE	6.41	7.91	7.26	31.10	21.78	25.78
Wind data source: Ground station						
Statistical metrics	Altitude [m]			Direction [°]		
	Non-hovering	Hovering	Total	Non-hovering	Hovering	Total
RMSE	1,269.25	1,271.35	1,270.45	113.22	114.45	113.92
MAE	524.64	566.57	548.60	105.68	101.02	103.02

the UAV. This introduces a trade-off between flight speed and spatial coverage in non-hovering flight mode, where the UAV must fly slow enough to gather accurate concentration data but still cover a sufficient area during the flight.

In addition to affecting measurement accuracy, slower flight speeds also increase the time required to complete a single dataset. Although we assumed no significant temporal variation during dataset collection, flight operation with extremely slow speeds may introduce temporal fluctuations, especially over extended data collection periods. Therefore, maintaining an appropriate flight speed is necessary to ensure the timely completion of the dataset while minimizing the impact of temporal variation.

Validating the precision of CO_2 sensor measurements is essential to ensure the integrity of research findings. Fig. 5(b) illustrates that the background CO_2 concentrations, determined by averaging measurements from three planes out of four boundary planes where the plume was not detected across flight missions, were consistently within the range of 390 to 400 ppm for both the hovering and non-hovering flight modes. Such background levels of CO_2 correspond to the values reported in the previous studies (World Resources Institute, 2022; Lee et al., 2023), confirming the sensor reliability in accurately capturing ambient CO_2 concentrations in both flight modes. Moreover, the result indicated that non-hovering flights, notwithstanding their reduced efficacy in capturing peak CO_2 concentrations, effectively measure background CO_2 levels. Sensor performance validation was further conducted by comparing the peak CO_2 concentrations observed during each flight mission with the calculated plume center concentrations, as detailed in the SI Note S7.

3.3. Sensor responses to the air pollutants

The response time of the CO_2 sensor during field measurements was investigated to assess its impact on monitoring accuracy. Unsteady airflow and turbulence in the field can disrupt sensor intake, affecting the measurements. Although the sensor modules were positioned to minimize external influences, field conditions can still introduce variability, making it difficult to define a precise response time compared to controlled laboratory chamber conditions. In addition, quantifying the response time in the field is challenging because the exact moment when the sensor begins to detect the plume is unclear. Instead, we quantified the time it takes for the CO_2 concentration to rise from background levels to the plume detection threshold (approximately 800 ppm, defined as flight mission validation criterion) during hovering flights. This duration ranged from 2 to 8 s, with a mean of 3.4 s and a standard deviation of 1.7 s, providing an estimation that helps in understanding the field response time under real-world conditions.

This finding aligns with the broader sensor response time analysis performed in this study, further emphasizing the importance of response time in the detection of multiple air pollutants. The present

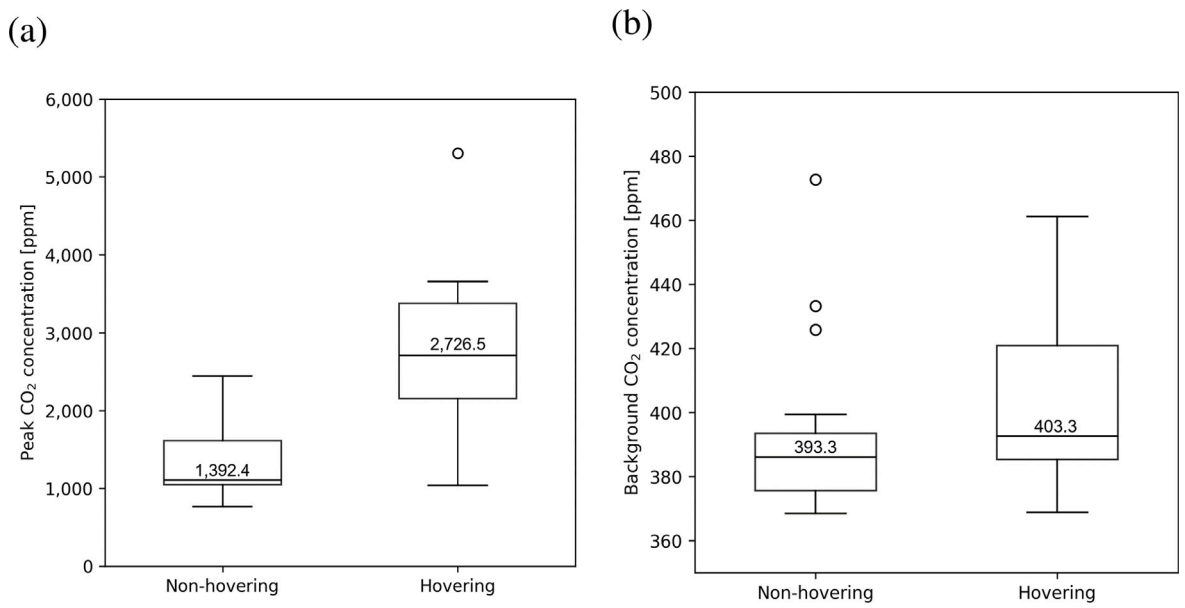

Fig. 5. Comparison of peak and background CO_2 concentrations in the hovering and non-hovering flight modes. Figure (a) presents the maximum CO_2 concentration recorded in each flight mission, categorized by hovering and non-hovering flight modes. Figure (b) presents the background CO_2 concentrations for flight modes, which were determined by averaging the measurements from boundary areas where the plume was not detected across flight missions.

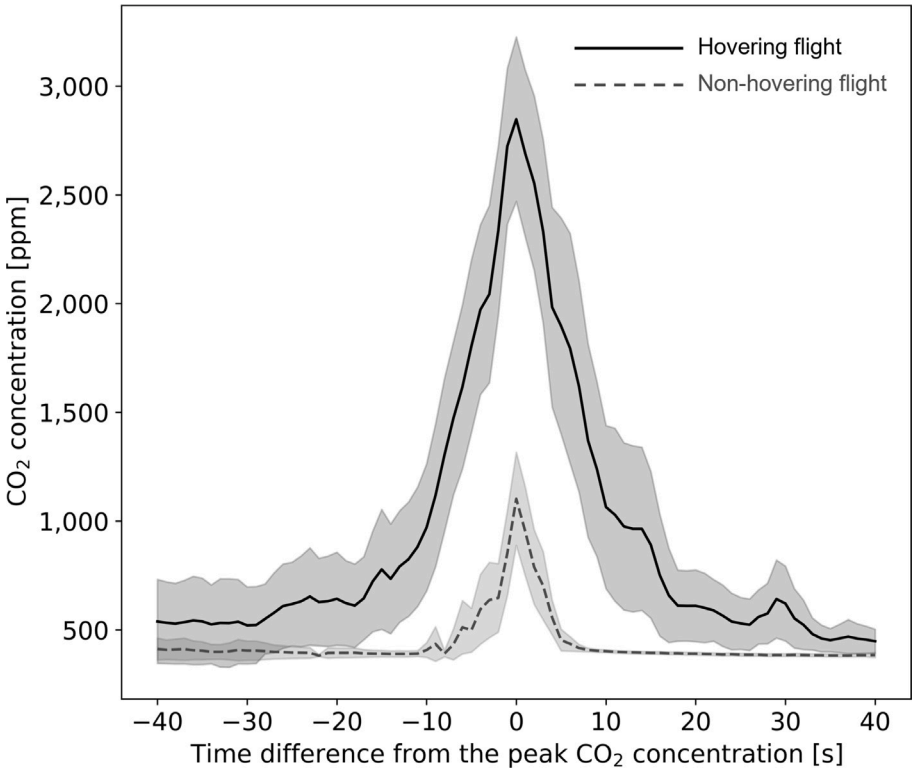

Fig. 6. Averaged time series of CO_2 concentrations surrounding the peak values for each flight mode over a 40-second window. The time series is illustrated with the 90% confidence interval represented as a shaded area beneath the curves.

study utilized sensor modules equipped with various air pollutant sensors (CO_2, CH_4, NO_2, CO, H_2S, PM_{10}, O_3, VOCs). This setup facilitated an exploration of sensor response times and their influence on monitoring results. Fig. 7 elucidates the disparities in sensor response times near the plume center during hovering flight missions, highlighting the swifter response of the CO_2 sensor compared to others. The variance in the sensor response times demonstrates the need for careful sensor selection in the design of UAV monitoring systems, especially when incorporating various sensor types to detect a wide range of pollutants. Several studies aim to monitor multiple pollutants using low-cost sensors through drone-based monitoring (Zhou et al., 2017; Rutkauskas et al., 2019). In such cases, electro-chemical low-cost sensors, in particular, might require careful consideration regarding their sensor response. Utilizing sensors with fast response times can enhance the efficiency of monitoring missions, which is crucial given the limited flight durations of UAVs.

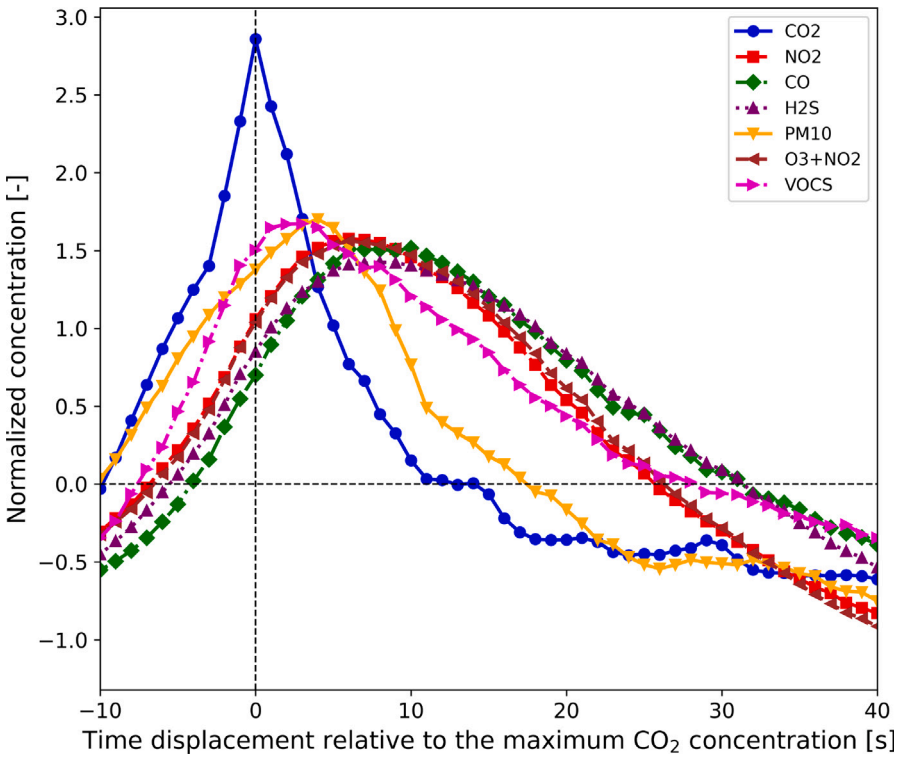

Fig. 7. Comparison of the sensor response dynamics across different pollutant sensors. Each curve illustrates the normalized time series of the average pollutant concentrations centered around the peak CO_2 values during hovering flight missions, covering a time window from −10 to 40 s. The moment of the maximum CO_2 concentration is aligned at time zero. Normalization was performed by subtracting the mean and dividing by the standard deviation of each sensor's data to facilitate cross-sensor comparison.

Additionally, the varying response times of the sensors highlight the necessity of determining the appropriate hovering duration of the UAVs to ensure accurate detection of all pollutants during comprehensive environmental monitoring missions within the constraints of UAV technology. Table S4 in the SI Note S8 compares the response times noted by the manufacturer and the observed discrepancies in peak concentration detection across pollutants from 15 hovering flight mode missions. The values illustrate deviations from laboratory-based specifications, emphasizing the need for empirical validation of sensor performance under field conditions rather than relying solely on manufacturer data. Therefore, a strategic approach to UAV flight planning, including preliminary field tests, must be determined to establish suitable hovering times that can encompass the different response times of multiple sensors under actual environmental conditions.

3.4. A hybrid monitoring approach at point sources

By comparing the measurement results from hovering and non-hovering flight modes, we identified the specific advantages and challenges in their effectiveness for localizing the plume centerline and measuring concentrations. Non-hovering flights, characterized by their swift execution and expansive coverage within the constraints of limited flight time, demonstrate equivalent proficiency in detecting the plume location when compared to hovering flights. However, they fall short in capturing high concentrations of CO_2. Hovering flights, on the other hand, are particularly effective at accurately measuring high concentrations of pollutants.

Based on these observations, we recommend a hybrid monitoring approach that combines plume localization via non-hovering flights, followed by detailed concentration measurements using hovering flights. Initially, a non-hovering flight would be deployed to quickly identify the general location and altitude of the plume. By measuring wind data near the point source for a short duration, the altitude of the plume center can be estimated using a plume-rise model and operational data from the point source, while the plume direction can be determined using wind direction data from a UAV-mounted anemometer. However, if operational data are unavailable at the target site, a boundary flight mission at a suitable altitude range can be an alternative solution to locate the plume center. In our experiments, a nine-layer non-hovering boundary flight provided extensive vertical coverage. Following the non-hovering flight mission, a targeted hovering flight would be implemented, focusing on the previously identified altitude for detailed and precise concentration measurements.

To evaluate the efficacy of the proposed hybrid flight strategy, we performed a validation analysis to ascertain whether the altitude and angular direction of the plume center maintained consistency across sequential non-hovering and hovering flights. Over five days of experimental runs, 10 sequential flight cases were analyzed, as depicted in Fig. 8. The interval between initiating the two flight modes averaged 32 min. Generally, within this interval range, the plume center's location remained stable across sequential flights. Statistical metrics indicate that the discrepancies between sequential flights were similar to those found in the comparison between model- and observation-based estimations of the plume center, as shown in Table 2. This consistency supports the viability of integrating non-hovering and hovering flights for enhanced accuracy of plume detection and concentration measurement. However, as the time interval increased, the location of the plume center identified during non-hovering flights significantly differed from that identified during hovering flights. The impact of temporal gaps between the two flight modes in the hybrid approach was further investigated and is presented in the SI Note S9.

Overall, this strategy combines the strengths of each flight mode while mitigating their limitations, offering a balanced method for UAV-based monitoring at a point source. It facilitates quick detection and thorough concentration measurement, making efficient use of UAVs for environmental monitoring within today's technological limits.

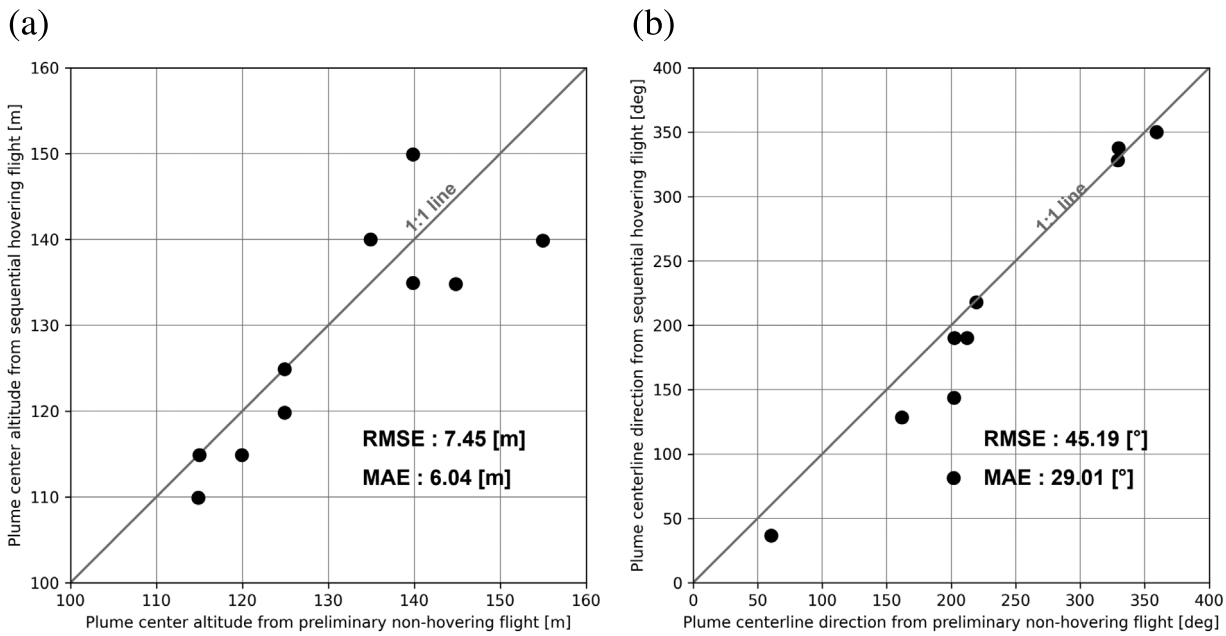

Fig. 8. Analytical comparison of plume center characteristics between initial non-hovering and subsequent hovering flights, showcasing (a) altitude variations and (b) directional shifts. The data points represent individual paired flight sessions, with linear regression lines and 90% prediction intervals demonstrating the consistency and reliability of plume center identification across 10 sequential cases. Statistical metrics were obtained from the analysis of plume center variability across sequential non-hovering and hovering flights.

4. Conclusion

In this study, we developed an effective UAV-based monitoring strategy for the plume detection from a point source. The presented approach demonstrated that incorporating a plume rise model with a UAV-mounted anemometer improves the wind measurement accuracy compared to traditional ground-based weather stations, thereby increasing the reliability of model-based plume localization. Extending this scalable method, future research should evaluate the applicability of the presented flight strategy to non-point source pollution (i.e., area source, mobile source).

A comparison between hovering and non-hovering flights revealed that hovering flights have better accuracy for measuring high CO_2 concentrations of pollutants from incinerator stacks, emphasizing sensor response times in UAV-based air pollution monitoring. Rapid sensor response is important for capturing the peak pollutant concentrations. In addition, our field experiments led to the proposal of a hybrid monitoring approach combining both hovering and non-hovering flights. Such a strategy balances swift plume localization with detailed concentration analysis at point sources.

One of the main challenges in UAV-based air quality monitoring is the limited flight time due to current battery technology, which affects the extent of continuous monitoring and data collection. To improve battery efficiency, employing lightweight yet highly accurate sensors is crucial to minimize the payload burden on UAVs. This highlights the need for ongoing improvements in sensor design and calibration to enhance measurement accuracy. Future research should focus on developing sensors with better sensitivity and faster response times.

Another key implication of the current research is the potential for UAV-based monitoring strategies to advance toward emission quantification. The ultimate goal of this strategy would be to not only detect pollutant concentrations but also accurately quantify emissions from various sources. To achieve this, better sensor technologies, improved data analysis methods, and effective flight strategies must be integrated to provide more accurate emission rates, supporting environmental regulatory compliance and pollution control efforts.

Lastly, developing comprehensive regulatory frameworks for UAV application in air quality research is vital to ensure the safe, ethical, and effective application of the technology. Establishing clear guidelines will support UAV operations, protect public and environmental health, and lay the groundwork for future advancements in UAV-based air quality monitoring. As the field of study evolves, such frameworks will be crucial in maximizing the benefits of UAV technology for air quality monitoring.

CRediT authorship contribution statement

Horim Kim: Writing – review & editing, Writing – original draft, Visualization, Validation, Software, Methodology, Investigation, Formal analysis, Conceptualization. **Keun Taek Kim:** Writing – review & editing, Writing – original draft, Visualization, Validation, Software, Methodology, Investigation, Formal analysis, Conceptualization. **Sangjae Jeong:** Writing – review & editing, Supervision, Methodology. **Young Su Lee:** Writing – review & editing, Supervision, Methodology. **Xin Zhao:** Writing – review & editing, Supervision. **Jae Young Kim:** Supervision, Project administration.

Funding

This research was supported by the National Research Foundation of Korea (NRF) grant funded by the Korean government (MSIT) (No. NRF-2020R1A2C1012899).

Declaration of competing interest

The authors declare the following financial interests/personal relationships which may be considered as potential competing interests: Jae Young Kim, Horim Kim, and Keun Taek Kim have patent #10-2024-0075523 pending to Seoul National University R&DB Foundation. If there are other authors, they declare that they have no known competing financial interests or personal relationships that could have appeared to influence the work reported in this paper.

Acknowledgments

The authors appreciate the technical support from the Institute of Construction and Environmental Engineering at Seoul National University.

Appendix A. Supplementary data

Supplementary material related to this article can be found online at https://doi.org/10.1016/j.atmosenv.2024.120924.

Data availability

Data will be made available on request.

References

Allen, G., Hollingsworth, P., Kabbabe, K., Pitt, J.R., Mead, M.I., Illingworth, S., Roberts, G., Bourn, M., Shallcross, D.E., Percival, C.J., 2019. The development and trial of an unmanned aerial system for the measurement of methane flux from landfill and greenhouse gas emission hotspots. Waste Manage. 87, 883–892. http://dx.doi.org/10.1016/j.wasman.2017.12.024.

Alvarado, M., Gonzalez, F., Erskine, P., Cliff, D., Heuff, D., 2017. A methodology to monitor airborne PM10 dust particles using a small unmanned aerial vehicle. Sensors 17 (2), 343.

Andersen, T., Vinkovic, K., de Vries, M., Kers, B., Necki, J., Swolkien, J., Roiger, A., Peters, W., Chen, H., 2021. Quantifying methane emissions from coal mining ventilation shafts using an unmanned aerial vehicle (UAV)-based active AirCore system. Atmos. Environ.: X 12, 100135.

Bergamaschi, P., Corazza, M., Karstens, U., Athanassiadou, M., Thompson, R.L., Pison, I., Manning, A.J., Bousquet, P., Segers, A., Vermeulen, A.T., Janssens-Maenhout, G., Schmidt, M., Ramonet, M., Meinhardt, F., Aalto, T., Haszpra, L., Moncrieff, J., Popa, M.E., Lowry, D., Steinbacher, M., Jordan, A., O'Doherty, S., Piacentino, S., Dlugokencky, E., 2015. Top-down estimates of European CH4 and N2O emissions based on four different inverse models. Atmos. Chem. Phys. 15, 715–736. http://dx.doi.org/10.5194/acp-15-715-2015.

Bogner, J., Pipatti, R., Hashimoto, S., Diaz, C., Mareckova, K., Diaz, L., Kjeldsen, P., Monni, S., Faaij, A., Gao, Q., et al., 2008. Mitigation of global greenhouse gas emissions from waste: conclusions and strategies from the intergovernmental panel on climate change (IPCC) fourth assessment report. Working group III (mitigation). Waste Manag. Res. 26 (1), 11–32.

Briggs, G.A., 1984. Plume rise and buoyancy effects. In: Randerson, D. (Ed.), Atmospheric Science and Power Production. U.S. Department of Energy, Springfield, U.S.A., pp. 327–366, DOE/TIC 27601.

Brown, J.A., Harrison, M.R., Rufael, T., Roman-White, S.A., Ross, G.B., George, F.C., Zimmerle, D., 2023. Informing methane emissions inventories using facility aerial measurements at midstream natural gas facilities. Environ. Sci. Technol. 57 (39), 14539–14547.

Burgués, J., Marco, S., 2020. Environmental chemical sensing using small drones: A review. Sci. Total Environ. 748, http://dx.doi.org/10.1016/j.scitotenv.2020.141172.

Chen, Z., Jacob, D.J., Nesser, H., Sulprizio, M.P., Lorente, A., Varon, D.J., Lu, X., Shen, L., Qu, Z., Penn, E., Yu, X., 2022. Methane emissions from China: a high-resolution inversion of TROPOMI satellite observations. Atmos. Chem. Phys. 22, 10809–10826. http://dx.doi.org/10.5194/acp-22-10809-2022.

Finn, D., Carter, R.G., Eckman, R.M., Rich, J.D., Gao, Z., Liu, H., 2018. Plume dispersion in low-wind-speed conditions during project sagebrush phase 2, with emphasis on concentration variability. Bound.-Layer Meteorol. 169, 67–91. http://dx.doi.org/10.1007/s10546-018-0360-8.

Gålfalk, M., Nilsson Påledal, S., Bastviken, D., 2021. Sensitive drone mapping of methane emissions without the need for supplementary ground-based measurements. ACS Earth Space Chem. 5 (10), 2668–2676.

Google Earth Pro 7.3.6.9750, 2024. A satellite imagery of incinerator plant and its surroundings, Republic of Korea, 37.258746°, 127.065317°, eye altitude 712 m. Airbus, URL https://earth.google.com/web/. (Accessed 14 February 2024).

Han, T., Xie, C., Liu, Y., Yang, Y., Zhang, Y., Huang, Y., Gao, X., Zhang, X., Bao, F., Li, S.-M., 2024. Development of a continuous UAV-mounted air sampler and application to the quantification of CO 2 and CH 4 emissions from a major coking plant. Atmos. Meas. Tech. 17 (2), 677–691.

IPCC, 2006. In: Eggleston, H.S., Buendia, L., Miwa, K., Ngara, T., K., T. (Eds.), 2006 IPCC Guidelines for National Greenhouse Gas Inventories. Institute for Global Environmental Strategies (IGES), Hayama, Japan, Hayama, Kanagawa, Japan, URL http://www.ipcc-nggip.iges.or.jp, Prepared by the National Greenhouse Gas Inventories Programme.

Kuantama, E., Tarca, R., Dzitac, S., Dzitac, I., Vesselenyi, T., Tarca, I., 2019. The design and experimental development of air scanning using a sniffer quadcopter. Sensors 19 (18), 3849.

Kuuluvainen, H., Poikkimäki, M., Järvinen, A., Kuula, J., Irjala, M., Dal Maso, M., Keskinen, J., Timonen, H., Niemi, J.V., Rönkkö, T., 2018. Vertical profiles of lung deposited surface area concentration of particulate matter measured with a drone in a street canyon. Environ. Pollut. 241, 96–105.

Lee, H., Calvin, K., Dasgupta, D., Krinner, G., Mukherji, A., Thorne, P., Trisos, C., Romero, J., Aldunce, P., Barrett, K., et al., 2023. Climate Change 2023: Synthesis Report. Contribution of Working Groups I, II and III to the Sixth Assessment Report of the Intergovernmental Panel on Climate Change. The Australian National University.

Li, J., Yu, X.B., 2018. Onshore and offshore wind energy potential assessment near lake erie shoreline: A spatial and temporal analysis. Energy 147, 1092–1107. http://dx.doi.org/10.1016/j.energy.2018.01.118.

Lu, X., Jacob, D.J., Wang, H., Maasakkers, J.D., Zhang, Y., Scarpelli, T.R., Shen, L., Qu, Z., Sulprizio, M.P., Nesser, H., Bloom, A.A., Ma, S., Worden, J.R., Fan, S., Parker, R.J., Boesch, H., Gautam, R., Gordon, D., Moran, M.D., Reuland, F., Villasana, C.A., Andrews, A., 2022a. Methane emissions in the United States, Canada, and Mexico: evaluation of national methane emission inventories and 2010–2017 sectoral trends by inverse analysis of in situ (GLOBALVIEWplus CH4 ObsPack) and satellite (GOSAT) atmospheric observations. Atmos. Chem. Phys. 22, 395–418. http://dx.doi.org/10.5194/acp-22-395-2022.

Lu, H., Xie, M., Liu, X., Liu, B., Liu, C., Zhao, X., Du, Q., Wu, Z., Gao, Y., Xu, L., 2022b. Spatial-temporal characteristics of particulate matters and different formation mechanisms of four typical haze cases in a mountain city. Atmos. Environ. 269, http://dx.doi.org/10.1016/j.atmosenv.2021.118868.

Ma, Y., Ye, J., Ribeiro, I.O., de Arellano, J.V.-G., Xin, J., Zhang, W., de Souza, R.A.F., Martin, S.T., 2021. Optimization and representativeness of atmospheric chemical sampling by hovering unmanned aerial vehicles over tropical forests. Earth Space Sci. 8, http://dx.doi.org/10.1029/2020EA001335.

Mønster, J., Kjeldsen, P., Scheutz, C., 2019. Methodologies for measuring fugitive methane emissions from landfills – A review. Waste Manage. 87, 835–859. http://dx.doi.org/10.1016/j.wasman.2018.12.047.

Newman, S., Xu, X., Gurney, K.R., Hsu, Y.K., Li, K.F., Jiang, X., Keeling, R., Feng, S., O'Keefe, D., Patarasuk, R., Wong, K.W., Rao, P., Fischer, M.L., Yung, Y.L., 2016. Toward consistency between trends in bottom-up CO2 emissions and top-down atmospheric measurements in the los angeles megacity. Atmos. Chem. Phys. 16, 3843–3863. http://dx.doi.org/10.5194/acp-16-3843-2016.

Oosedo, A., Abiko, S., Konno, A., Uchiyama, M., 2017. Optimal transition from hovering to level-flight of a quadrotor tail-sitter UAV. Auton. Robots 41, 1143–1159.

Park, K., Lee, J., 2024. Mitigating air and noise pollution through highway capping: The bundang-suseo highway cap project case study. Environ. Pollut. 346, 123620.

Reuter, M., Bovensmann, H., Buchwitz, M., Borchardt, J., Krautwurst, S., Gerilowski, K., Lindauer, M., Kubistin, D., Burrows, J.P., 2021. Development of a small unmanned aircraft system to derive CO2 emissions of anthropogenic point sources. Atmos. Meas. Tech. 14 (1), 153–172.

Ripple, W.J., Wolf, C., Gregg, J.W., Levin, K., Rockström, J., Newsome, T.M., Betts, M.G., Huq, S., Law, B.E., Kemp, L., Kalmus, P., Lenton, T.M., 2022. World Scientists' Warning of a Climate Emergency 2022. BioScience 72 (12), 1149–1155. http://dx.doi.org/10.1093/biosci/biac083.

Rüdiger, J., Tirpitz, J.-L., De Moor, J.M., Bobrowski, N., Gutmann, A., Liuzzo, M., Ibarra, M., Hoffmann, T., 2018. Implementation of electrochemical, optical and denuder-based sensors and sampling techniques on UAV for volcanic gas measurements: Examples from masaya, turrialba and stromboli volcanoes. Atmos. Meas. Tech. 11 (4), 2441–2457.

Rutkauskas, M., Asenov, M., Ramamoorthy, S., Reid, D.T., 2019. Autonomous multi-species environmental gas sensing using drone-based Fourier-transform infrared spectroscopy. Opt. Express 27, 9578. http://dx.doi.org/10.1364/OE.27.009578, URL https://opg.optica.org/abstract.cfm?URI=oe-27-7-9578.

Seinfeld, J.H., Pandis, S.N., 2016. Atmospheric Chemistry and Physics: from Air Pollution to Climate Change. John Wiley & Sons.

Sekula, P., Bokwa, A., Bartyzel, J., Bochenek, B., Chmura, L., Galkowski, M., Zimnoch, M., 2021. Measurement report: Effect of wind shear on PM10 concentration vertical structure in the urban boundary layer in a complex terrain. Atmos. Chem. Phys. 21, 12113–12139. http://dx.doi.org/10.5194/acp-21-12113-2021.

Shah, A., Pitt, J.R., Ricketts, H., Leen, J.B., Williams, P.I., Kabbabe, K., Gallagher, M.W., Allen, G., 2020. Testing the near-field Gaussian plume inversion flux quantification technique using unmanned aerial vehicle sampling. Atmos. Meas. Tech. 13 (3), 1467–1484.

UNFCCC, 2007. Greenhouse gas inventory data.

U.S. Environmental Protection Agency, 1995. User's Guide for the Industrial Source Complex (ISC3) Dispersion Models: Volume II, Description of Model Algorithms. Technical Report EPA-454/B-95-003b; EPA-68-D3-0032, U.S. Environmental Protection Agency.

U.S. Environmental Protection Agency, 2023. AERMOD Model Formulation. Technical Report EPA-454/B-23-010, Office of Air Quality Planning and Standards, Air Quality Assessment Division, Research Triangle Park, NC.

U.S. Environmental Protection Agency, 2024. Draft Inventory of U.S. Greenhouse Gas Emissions and Sinks: 1990–2022. Technical Report EPA 430-D-24-001, U.S. Environmental Protection Agency, URL https://www.epa.gov/ghgemissions/draft-inventory-us-greenhouse-gas-emissions-and-sinks-1990-2022. (Accessed 19 March 2024).

Villa, T.F., Jayaratne, E.R., Gonzalez, L.F., Morawska, L., 2017. Determination of the vertical profile of particle number concentration adjacent to a motorway using an unmanned aerial vehicle. Environ. Pollut. 230, 134–142.

Vinković, K., Andersen, T., de Vries, M., Kers, B., van Heuven, S., Peters, W., Hensen, A., van den Bulk, P., Chen, H., 2022. Evaluating the use of an unmanned aerial vehicle (UAV)-based active AirCore system to quantify methane emissions from dairy cows. Sci. Total Environ. 831, 154898.

World Resources Institute, 2022. Climate watch historical GHG emissions. URL https://www.climatewatchdata.org/ghg-emissions. (Accessed 19 March 2024).

Zhao, T., Yang, D., Guo, D., Wang, Y., Yao, L., Ren, X., Fan, M., Cai, Z., Wu, K., Liu, Y., 2024. Low-cost UAV coordinated carbon observation network: carbon dioxide measurement with multiple UAVs. Atmos. Environ. 120609.

Zhou, X., Aurell, J., Mitchell, W., Tabor, D., Gullett, B., 2017. A small, lightweight multipollutant sensor system for ground-mobile and aerial emission sampling from open area sources. Atmos. Environ. 154, 31–41. http://dx.doi.org/10.1016/j.atmosenv.2017.01.029.